PHYSICAL REVIEW E **71**, 015403(R) (2005)

Electron acceleration by a nonlinear wakefield generated by ultrashort (23-fs) high-peak-power laser pulses in plasma

M. Kando,[1,*] S. Masuda,[1] A. Zhidkov,[2] A. Yamazaki,[1,†] H. Kotaki,[1] S. Kondo,[1] T. Homma,[1] S. Kanazawa,[1] K. Nakajima,[1,‡] Y. Hayashi,[1] M. Mori,[1] H. Kiriyama,[1] Y. Akahane,[1] N. Inoue,[1] H. Ueda,[1] Y. Nakai,[1] K. Tsuji,[1] Y. Yamamoto,[1] K. Yamakawa,[1] J. Koga,[1] T. Hosokai,[3] M. Uesaka,[3] and T. Tajima[1]

[1]*Advanced Photon Research Center, Kansai Research Establishment, Japan Atomic Energy Research Institute, 8-1 Umemidai, Kizu, Souraku, Kyoto 619-0215, Japan*

[2]*Department of Accelerator Physics and Engineering, National Institute of Radiological Sciences, 4-9-1 Anagawa, Inage, Chiba, 263-8555, Japan*

[3]*Nuclear Engineering Research Laboratory, The University of Tokyo, 2-22 Shirakata-shirane, Tokai, Naka, Ibaraki 319-1188, Japan*

(Received 28 May 2004; published 26 January 2005)

We study experimentally the interaction of the shortest at present (23-fs), relativistically intense (20-TW), tightly focused laser pulses with underdense plasma. MeV electrons constitute a two-temperature distribution due to different plasma wave-breaking processes at a plasma density of 10^{20} cm^{-3}. These two groups of electrons are shown numerically to constitute bunches with very distinctive time durations.

DOI: 10.1103/PhysRevE.71.015403 PACS number(s): 52.38.Kd, 52.35.Mw

Generation of very short, tens of MeV electron beams via laser wakefield acceleration (LWFA) [1] has been intensively studied in the last decade [2–14]. Various regimes of acceleration for background plasma electron injection such as laser-pulse self-modulation [3–7], forced laser acceleration [8], plasma wave breaking [9–11], direct laser acceleration [12], stochastic acceleration [13], and beat-wave acceleration [14] have been already investigated both experimentally and theoretically. However, these experiments have been carried out under the condition $c\tau > \lambda_p$, where c is the speed of light, τ is the laser-pulse duration, $\lambda_p = 2\pi c/\omega_{pl}$ is the plasma wavelength, and ω_{pl} is the plasma frequency. Nowadays, the duration of laser pulses with powers of the order of a PW can be considerably reduced down to 10–20 fs [15,16]. This opens the way to both studying LWFA far from the regime of self-modulation, which is not the dominant acceleration process in short pulse lasers, and reducing the effects of laser-pulse duration on the plasma relaxation. Since our laser-pulse length becomes equal to the plasma wavelength at atmospheric pressure, both strong depletion of the pulse and strong plasma wave breaking are expected at $c\tau < \lambda_p$ [17].

In this Rapid Communication, we report the results of charge and energy distribution measurements for electrons accelerated during the interaction of a short laser pulse (23 fs) tightly focused into an underdense plasma. In the high-density regime, we found a two-temperature distribution of accelerated electrons. With the help of numerical simulations, we attribute these two groups of electrons to different wave-breaking mechanisms. In the $c\tau < \lambda_p$ regime, which partly satisfies the predicted self-injection condition [17], we have observed nonmonotonic behavior of the total electron charge with increase of the plasma density.

We use a 100-TW, 20-fs, 800-nm, and 10-Hz Ti:sapphire laser system based on chirped pulse amplification [15] at the Advanced Photon Research Center, Japan Atomic Energy Research Institute. At present, a 20-TW, 23-fs laser pulse is focused onto a gas target with an off-axis parabolic mirror with a focal length of 178 mm ($f/3.5$). The experimental set up is depicted in Fig. 1. The laser-pulse energy is measured with a calibrated pyroelectric joulemeter and the typical total energy is 420 mJ. The focus spot size is measured by use of image-relay optics with a magnification of 100 and is 10 μm at $1/e^2$ containing 50% of the total laser-pulse energy. This corresponds to the peak focused intensity of 2.3×10^{19} W/cm^2. The contrast ratio of the laser system is typically 10^{-6} on the nanosecond scale. A specially designed pulsed valve with a shock-wave-free nozzle is used to form a flat-top-profile helium gas plume in a vacuum chamber. The nozzle has a rectangular shape of 1.3×4 mm. A detailed description of the pulsed valve and density measurements will be available in a forthcoming paper. The plasma density is varied from 1×10^{19} to 1.4×10^{20} cm^{-3} (minimum $\lambda_p/c\tau = 0.4$) in fully ionized helium by changing the stagnation pressure of the pulsed valve. The position of the gas jet is aligned carefully in such a way that the electron signal becomes its maximum by adjusting movable stages equipped with the gas jet. The laser is focused at a point 1 mm from

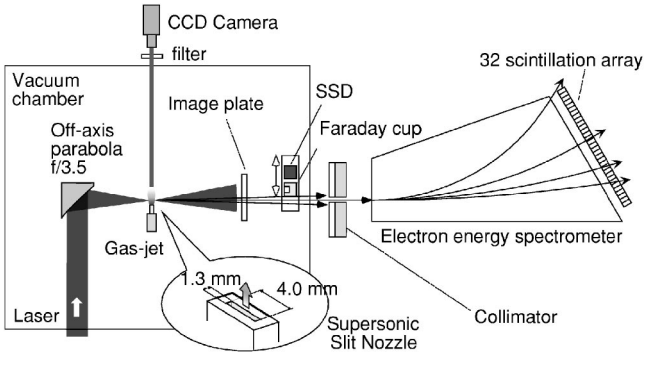

FIG. 1. A schematic of the experimental set up.

*Electronic address: kando@apr.jaeri.go.jp

†Also at Institute for Chemical Research, Gokasho, Uji, Kyoto 611-0011, Japan.

‡Also at High Energy Accelerator Research Organization (KEK), 1-1 Oho, Tsukuba, Ibaraki 305-0801, Japan.

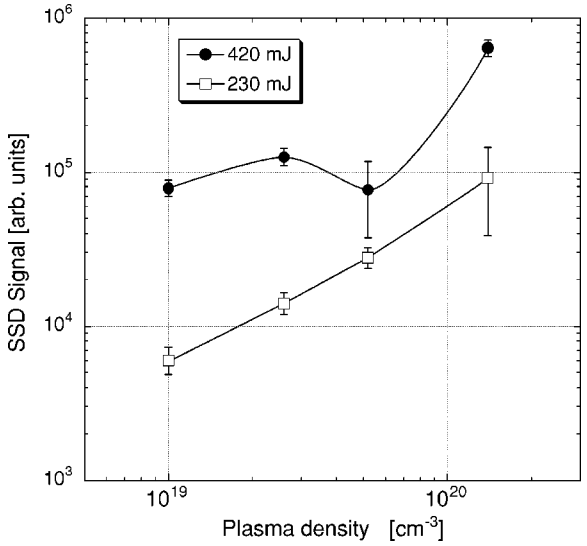

FIG. 2. Electron signal for different plasma densities for two laser-pulse energies.

the entrance edge of the slit. The gas jet is operated at a repetition rate of 0.5–5 Hz.

Energetic electrons are monitored with a lithium-doped silicon semiconductor detector (SSD) with amplifiers. To avoid exposure from the strong laser light and plasma fluorescence, the SSD is contained in a shielding box which has an entrance window covered with a 20-μm-thick titanium foil. The electron spatial distribution is measured with a stack of four image plates (Fuji Film, BAS-SR) with shielding substrates to measure rough electron energies in the image plates. The image plates are placed 180 mm from the focus on the laser axis. The electron charge is measured with a Faraday cup consisting of 20×20 mm copper, signals of which are taken with a CAMAC charge-sensitive analog-to-digital converter (ADC) module. The electron energy spectrum is measured with a magnetic spectrometer composed of a dipole magnet and a 32-channel plastic scintillation array coupled with photomultipliers. In order to increase energy resolution, a collimator is placed in front of the dipole magnet which limits the electron beam acceptance to within ±10 mrad. The collimator is made of a stack of polyethylene and lead to reduce the amount of bremsstrahlung x rays hitting the plastic scintillation array. Lead shielding blocks are also placed around the scintillation detectors to reduce noise from x rays. Each scintillator is calibrated to output the same signal height using a beta-decay source (^{90}Sr-^{90}Y).

A charge-coupled device (CCD) camera with a gate time of 4 ms is placed perpendicularly to both the laser propagation and polarization directions to observe light emissions from the focus point. Two kinds of bandpass filters are placed between the focus point and the CCD camera to limit the light wavelength. A bluepass filter is set to measure plasma recombination fluorescence and a redpass filter is used to measure wavelengths greater than 726 nm, while the laser bandwidth is 100 nm centered at 800 nm.

A plasma density scan is shown in Fig. 2 for laser energies of 230 and 420 mJ corresponding to intensities of $I=1\times10^{19}$ and 2×10^{19} W/cm^2, respectively. One can see very

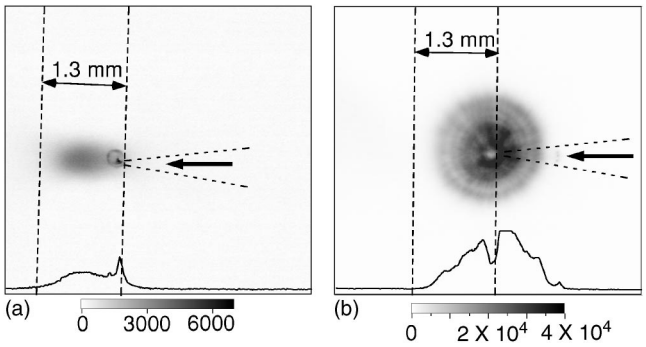

FIG. 3. Plasma and scattered light images at a plasma density of 1.4×10^{20} cm^{-3} and an intensity of 2.3×10^{19} W/cm^2 taken with a CCD camera with a bluepass (410–532 nm) filter (a) and a redpass (>732 nm) filter (b).

rapid growth of the electron signal with the laser intensity, almost an order of magnitude. At the lower intensity, we observe a monotonic increase in the electron signal with the plasma density. In contrast, the signal reaches its first maximum around the resonant density $N_e=2.5\times10^{19}$ cm^{-3} at the higher intensity. Here, the resonant density for LWFA including relativistic correction is given by $N_{res}=\pi(1+a_0^2/2)^{1/4}/(r_e\sigma_z^2)$, where a_0 is the normalized vector potential of the laser, r_e is the classical electron radius, and σ_z is the standard deviation of the pulse length assuming a Gaussian temporal laser profile.

The measured electron charge of accelerated electrons is 5 nC (3×10^{10}) per shot at the Faraday cup. The solid angle of the Faraday cup is 0.012 sr, therefore, the total amount of the accelerated charge is extremely high. Assuming that this electron bunch length is on the order of the plasma wavelength, the peak current of the beam may be about 0.5 MA. The electron spot radius (r_1) at $L=180$ mm downstream from the focus is measured to be 30 mm with the image plate. Assuming that the electron beam spot, r_0, at the focus is the same as that of the laser and collimated at the focus, the unnormalized emittance, ε, can be calculated by $\varepsilon=(r_0/L)\sqrt{r_1^2-r_0^2}$. Thus, the emittance is estimated to be 0.5 π mm mrad, where no space-charge effects are included in this calculation.

Present measurements are not free from the effect of the laser prepulse. To show this effect we took a snapshot of the plasma image by the use of several filters. The plasma recombination fluorescence image obtained with the bluepass filter is shown in Fig. 3(a). A broad, weak ellipse shape image is seen and a strong peak is located at around the laser focus. An image produced with the redpass filter is shown in Fig. 3(b). In contrast to the peak in Fig. 3(a), the corresponding point becomes a valley. Because the redpass filter transmits light close to the laser wavelength, this image represents the scattered or reflected laser light and, hence, displays a very short time scale (~20 fs). One possible interpretation is a formation of cavity around the focus, at which the laser lights are reflected. A scenario of the formation of the cavity has been reported under effects of a prepulse [9]. A cavity is clearly seen in the reflected light image (the lighter regions correspond to lower plasma density) so that effects with re-

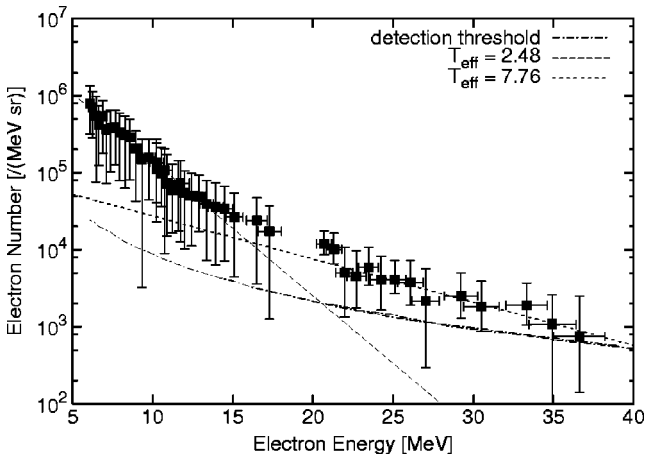

FIG. 4. Energy spectrum obtained at a plasma density of 1.4×10^{20} cm^{-3} and a laser intensity of 10^{19} W/cm^2. The dashed line shows the detection threshold which corresponds to the energy deposited by a relativistic electron entering each detector. By changing the magnetic-field strength and shielding in front of the detectors, we confirm that these signals are due to high-energy electrons. Exponential fit curves are also plotted, the effective temperatures of which lead to 2.5 and 7.8 MeV, respectively.

gard to shock-wave formation by the laser have to be taken into account [9]. Since in the present experiment the intensity of the ns prepulse is of the order of 10^{13} W/cm^2, the prepulse forms a preformed plasma and is absorbed through an inverse bremsstrahlung process. It is reasonable to assume that density steepening takes place and a cavity is formed before the arrival of the intense main pulse. A hydrodynamic simulation similar to that done in Ref. [9] shows that a cavity with length $\sim$180 μm and a shock wave with maximum density $N_e=3.5\times10^{20}$ cm^{-3}, and density gradient along the laser propagation axis $[d\ln(N_e)/dx]^{-1}\sim5$ μm, is formed after 2-ns prepulse irradiation under the conditions of Fig. 3.

Though the observed maximum in the electron charge requires further special investigation, the high-density results have to follow the well-known scenario of a wave-breaking process [11,18]. For this reason we performed detailed measurements of the electron spectrum for the high-density plasma along with two-dimensional (2D) particle-in-cell simulation. The measured energy spectrum at a plasma density of $N_e=1.4\times10^{20}$ cm^{-3}, is shown in Fig. 4. The data points are averaged over 100 shots and error bars show the maximum and minimum limits. We performed a two-dimensional PIC simulation using the moving-window technique [9] for laser pulses where $\lambda=0.78$ μm with mobile He ions. The whole plasma length is set to 1.3 mm, with a density gradient of length 5 μm along the laser propagation axis at the entrance edge of the gas jet. The gradient was chosen to agree with that obtained from the 2D hydrodynamic simulation. In the 2D PIC simulation, we use 16 particles per cell in a 160×120 μm (2800×2048 cells) window which moves at the speed of light. The laser pulse has a duration of 23 fs at full width at half maximum (FWHM) and an intensity of $I=2\times10^{19}$ W/cm^2. The electron energy distribution obtained in the calculation [Fig. 5(a)] reproduced fairly well the experimental one (Fig. 4). The two groups of electrons with different temperatures, $T_1\sim8$ MeV and $T_2\sim2.2$ MeV, are reproduced well. According to the spatial distribution of the electron momentum in the 2D simulation, these groups have different temporal duration, see Fig. 5(b). The higher temperature group constitutes a bunch with duration around 40 fs while the colder electron group has a length comparable to (or may be longer than) the simulation window which is 160 μm or 0.53 ps. According to the calculation, the shorter bunch consists of electrons injected at the shock-wave front and further accelerated by the plasma wakefield behind the laser pulse. The longer bunch is formed by electrons injected and accelerated by the wave breaking of the plasma wakefield in the uniform part of the plasma. Since the latter process lasts much longer than the injection at the front of the shock wave, the duration of the corresponding bunch is also longer. Because there is no practical method to separate these two groups of electrons, this parasitic process may seriously restrict application of such electrons in femtosecond measurements, and, hence, requires detailed study.

In conclusion, we have measured accelerated electrons produced in the interaction of the shortest at present, 23-fs, relativistically intense, 20-TW, tightly focused laser pulses with underdense He plasma. Strong nonmonotonic behavior of the total charge of accelerated electrons near the resonant plasma density has been observed. A 5-nC total charge of accelerated electrons with an emittance of 0.5 π mm mrad has been detected at higher plasma density. A two-temperature distribution of accelerated electrons, $T_1\sim8$ MeV and $T_2\sim2.5$ MeV, has been found. We attribute this to the existence of different plasma wave-breaking processes: (i) rapid wave-breaking injection at the front of the shock wave produced by the laser prepulse with further elec-

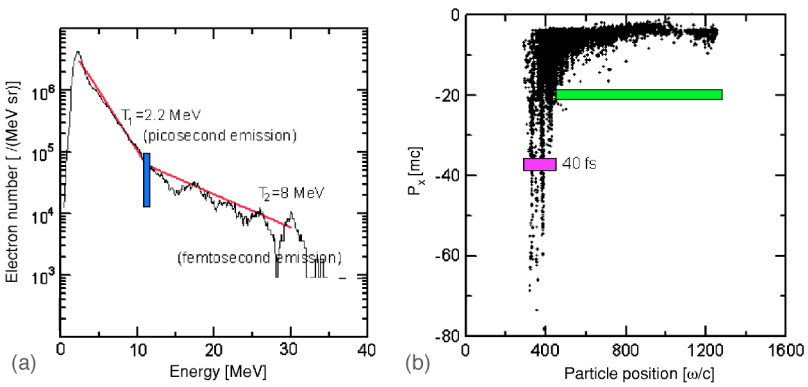

FIG. 5. (Color online) Electron energy spectrum (a) and spatial distribution of electron momentum (b) in the plasma with $N_e=1.4\times10^{20}$ cm^{-3} irradiated by a laser pulse with an intensity of $I=2\times10^{19}$ W/cm^2.

tron wakefield acceleration up to high energy and (ii) slower injection originating from the wave breaking in the uniform part of the plasma. The latter group of the electrons is shown numerically to constitute a bunch with a duration of about a picosecond.

The authors acknowledge T. Utsumi, A. Nagashima, T. Kimura, and Y. Kato for their encouragement. This research was partly supported by the Ministry of Education, Science, Sports and Culture, Grant-in-Aid for Specially Promoted Research No. 15002013.

[1] T. Tajima and J. M. Dawson, Phys. Rev. Lett. **43**, 267 (1979).
[2] E. Esarey, P. Sprangle, J. Krall, and A. Ting, IEEE Trans. Plasma Sci. **24**, 252 (1996).
[3] K. Nakajima *et al.*, Phys. Rev. Lett. **74**, 4428 (1995).
[4] D. Umstadter *et al.*, Science **273**, 472 (1996).
[5] C. I. Moore *et al.*, Phys. Rev. Lett. **79**, 3909 (1997).
[6] V. Malka *et al.*, Phys. Plasmas **79**, 2682 (2001).
[7] W. P. Leemans *et al.*, Phys. Plasmas **8**, 2510 (2001).
[8] V. Malka *et al.*, Science **298**, 1600 (2002).
[9] T. Hosokai *et al.*, Phys. Rev. E **67**, 036407 (2003).
[10] S. V. Bulanov, V. I. Kirsanov, and A. S. Sakharov, JETP Lett. **53**, 565 (1991).
[11] S. Bulanov, N. Naumova, F. Pegorano, and J. Sakai, Phys. Rev. E **58**, R5257 (1998).
[12] C. Gahn *et al.*, Phys. Rev. Lett. **83**, 4772 (1999); Phys. Plasmas **9**, 987 (2002).
[13] T. Nakamura, S. Kato, M. Tanimoto, and T. Kato, Phys. Plasmas **9**, 1801 (2002); M. Tanimoto *et al.*, Phys. Rev. E **68**, 026401 (2003).
[14] Y. Kitagawa *et al.*, Phys. Rev. Lett. **68**, 48 (1992).
[15] K. Yamakawa *et al.*, Opt. Lett. **12**, 1468 (1998).
[16] M. Aoyama *et al.*, Opt. Lett. **28**, 1594 (2003).
[17] A. Zhidkov, J. Koga, K. Kinoshita, and M. Uesaka, Phys. Rev. E **69**, 035401 (2004).
[18] R. G. Hemker, N. M. Hafz, and M. Uesaka, Phys. Rev. ST Accel. Beams **5**, 041301 (2002); P. Tomassini *et al.*, *ibid.* **6**, 121301 (2003).